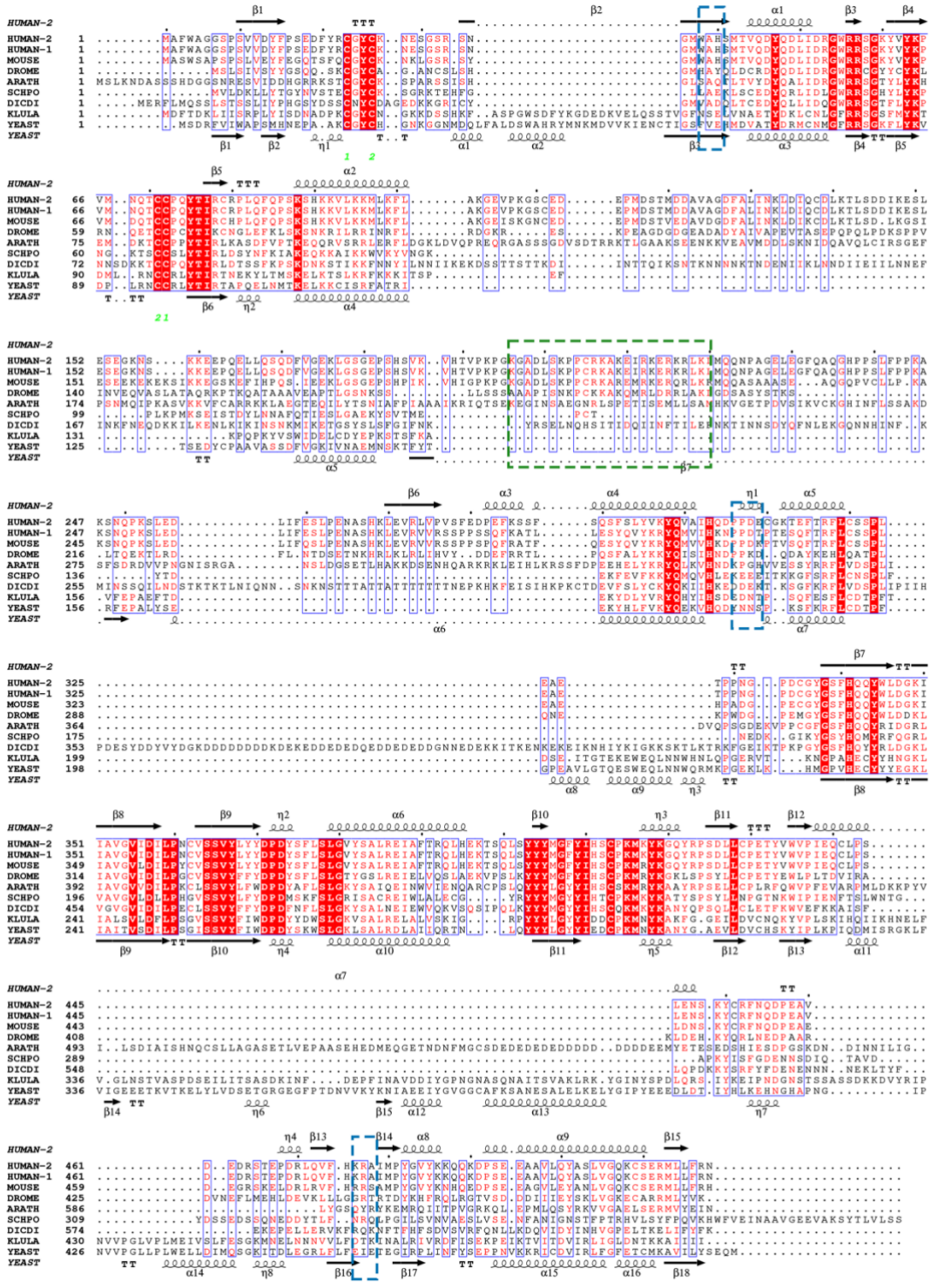

Supplementary Figure 1. Multiple sequence alignment of ATE1 sequences in Uniprot from model organisms (yeast, SCHPO, DICDI, ARATH, DROME, mouse, and isoforms 1 and 2 of human) using COBALT and displayed using ESPript3. Arrows and spirals indicate β-strands and α-helices, respectively. Red backgrounds and boxes indicate identical and similar residues.

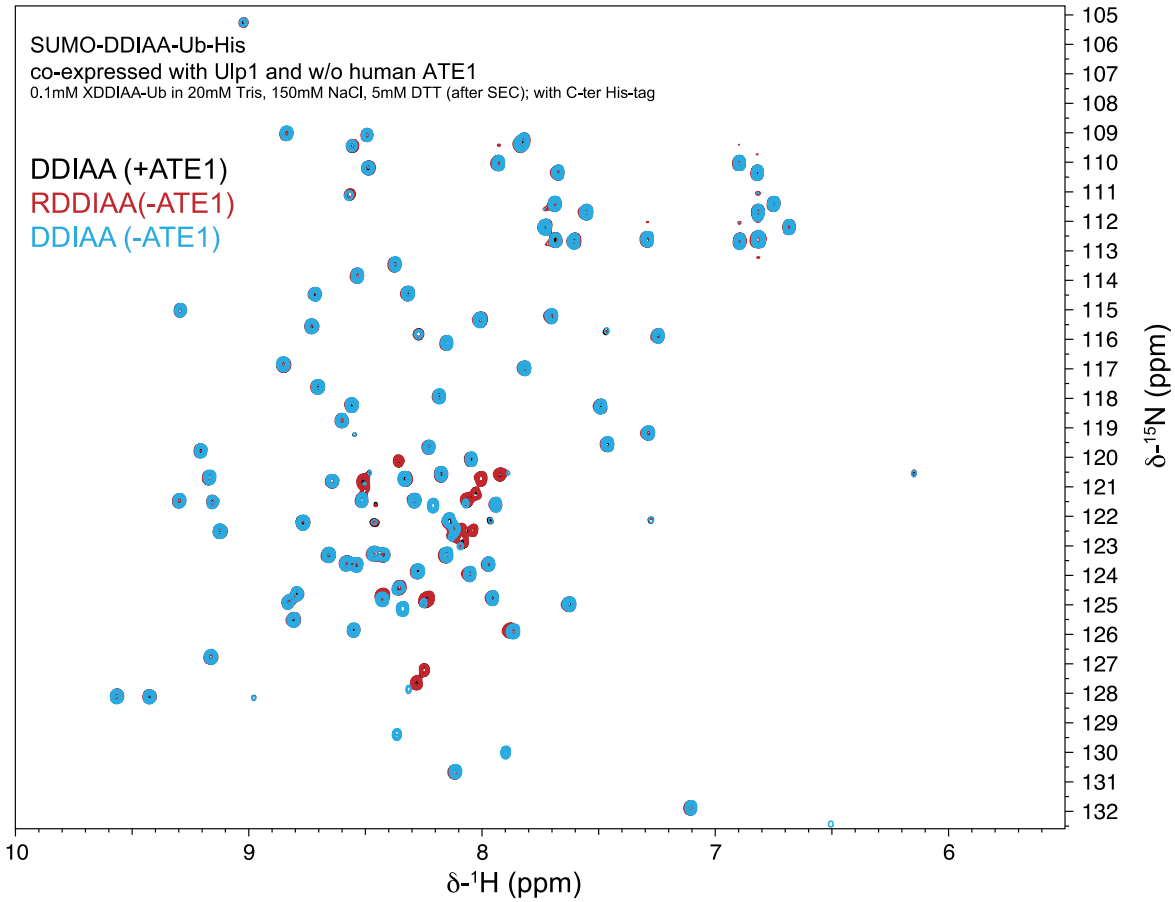

Supplementary Figure 2. Superimposed $^{1}H,^{15}N$ heteronuclear single quantum coherence (HSQC) spectra of the substrate DDIAA-Ub co-expressed with ATE1 (black) with recombinantly purified corresponding Nt-arginylated product RDDIAA-Ub (red) or unmodified DDIAA-Ub (blue) in the absence of ATE1.

Suppl. Fig. 3

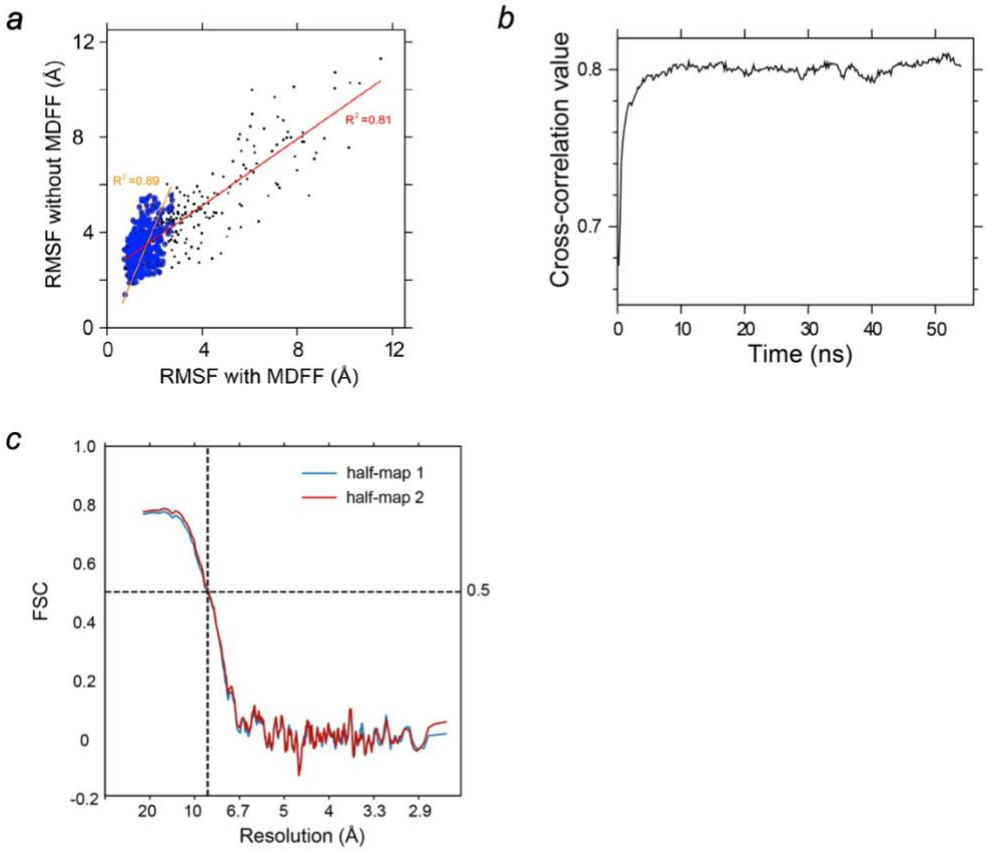

Supplementary Figure 3. MDFF structural validation. (a) Root-mean-square-fluctuation (RMSF) analysis of the ensemble with and without molecular dynamics flexible fitting (MDFF) for all residues in the full-length structure (black dots) and residues within cryoEM map (blue dots). Both comparisons show strong linear relationships with R2 of 0.81 (red line) and 0.89 (orange line), respectively. (b) Time evolution of cross-correlation value between structure model and cryoEM map. (c) FSC curves of the refined model versus half-map 1 (blue) or half-map 2 (red).

Suppl. Fig. 4

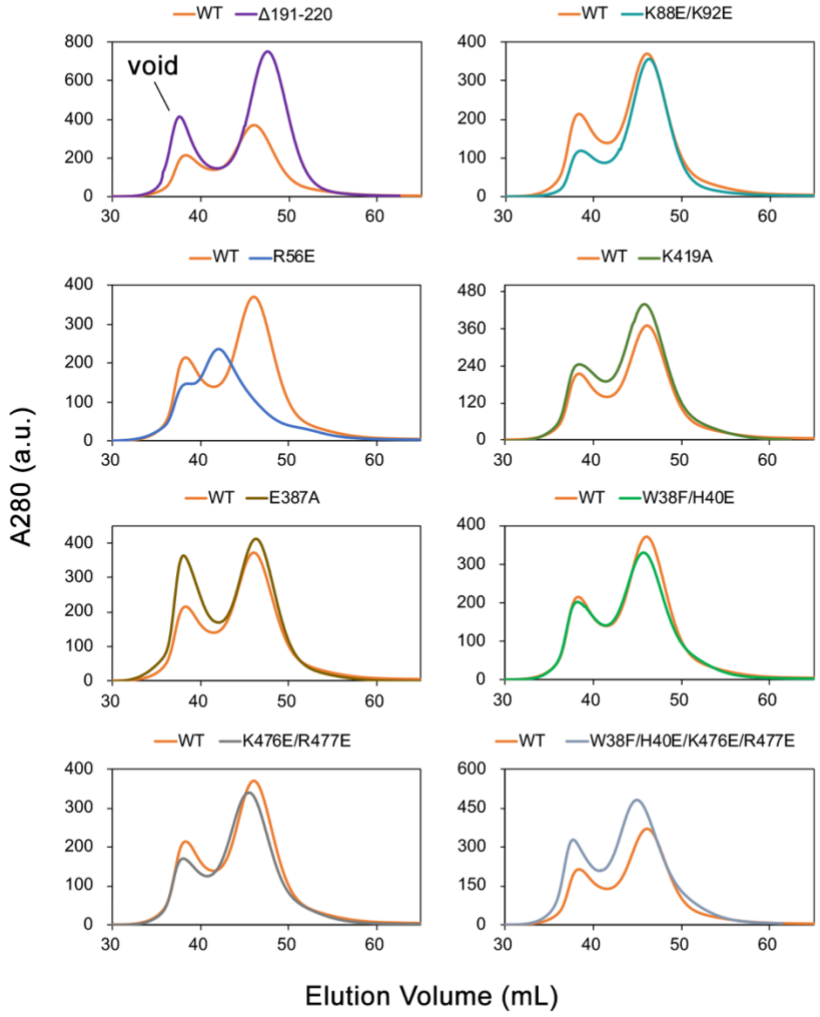

Supplementary Figure 4. Gel filtration profiles of WT and mutant ATE1 proteins.

Suppl. Fig. 5

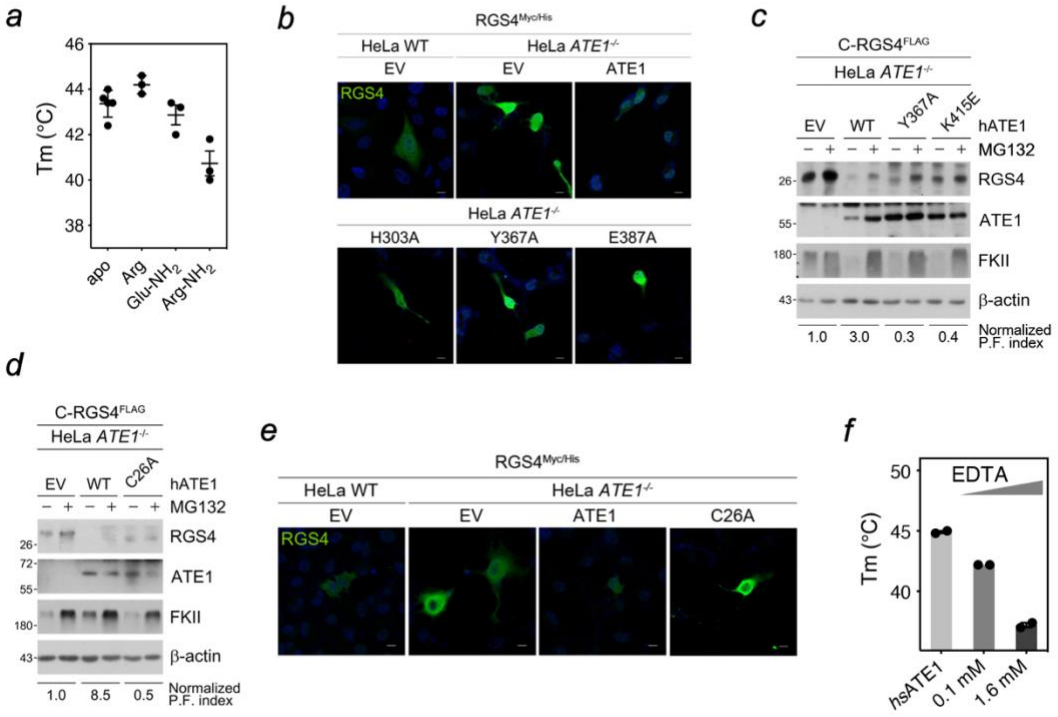

Supplementary Figure 5. Key residues required for ATE1 activity and stability. (a) T_m values derived from DSF for the ATE1 protein in the presence of Arg, Glu-NH_2, Arg-NH_2. Data are presented as mean values +/- SD. Error bars represent SD determined from at least three independent experiments (n=3 or 5). (b) Immunostaining analysis of recombinant RGS4-Myc/His with R56E, K415A, K419E, and wild-type hATE1 in WT or ATE1 deficient HeLa cells. Scale bar, 10 µm. (c,d) Immunoblotting analysis of exogenously expressed C-RGS4-FLAG in *ATE1*-deficient HeLa cells expressing WT and indicative ATE1 mutants with MG132 treatment (10 µM, 6 h). Proteasomal flux (P.F.) indices were calculated based on the ratio of RGS4 levels in the presence or absence of MG132. The samples were derived from the same experiment and the blots were processed in parallel. (e) Same as (b) but with C26A mutant of hATE1. (f) T_m values derived from DSF for the ATE1 protein in the presence of increasing amount of EDTA in duplicate measurements.

Suppl. Fig. 6

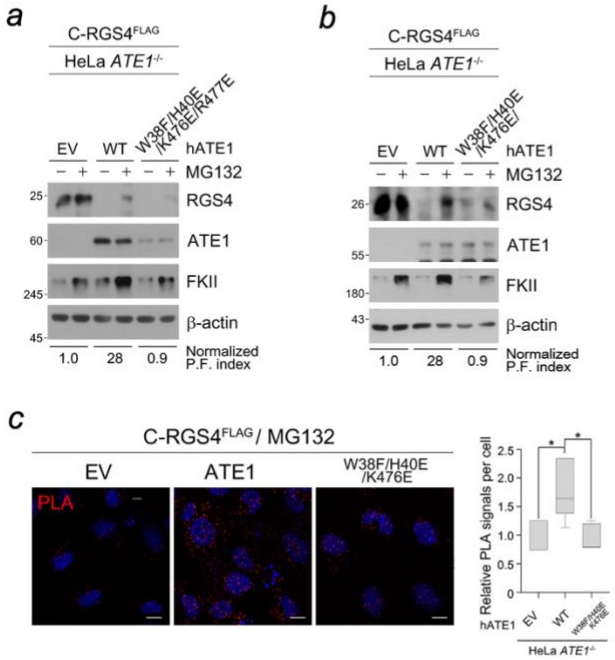

Supplementary Figure 6. Critical roles of residues at ATE1 dimeric interface for activity. (a) Western blotting of C-RGS4-FLAG and WT or mutant hATE1 ectopically expressed in *ATE1*$^{-/-}$ HeLa cells. The proteasomal fluxes of RGS4 with W38F/H40E/K476E/R477E quadruple mutant of hATE1 were compared with WT hATE1. (b) Same as (a) but with W38F/H40E/K476E triple mutant of hATE1. The samples were derived from the same experiment and the blots were processed in parallel. (c) PLA assay of recombinant C-RGS4-FLAG (PLUS) and W38F/H40E/K476E mutant of hATE1-2 (MINUS) in MG132 (10 μM, 6 h) treated *ATE1*$^{-/-}$ HeLa cells. Scale bar, 10 μm. Quantification is based on normalized PLA signal intensity (n=50 cells). Within each box, horizontal black lines denote median values; boxes extend from the 25th to the 75th percentile of each group's distribution of values; vertical extending lines denote adjacent values. *p<0.05 using the paired t-test.

Suppl. Fig. 7

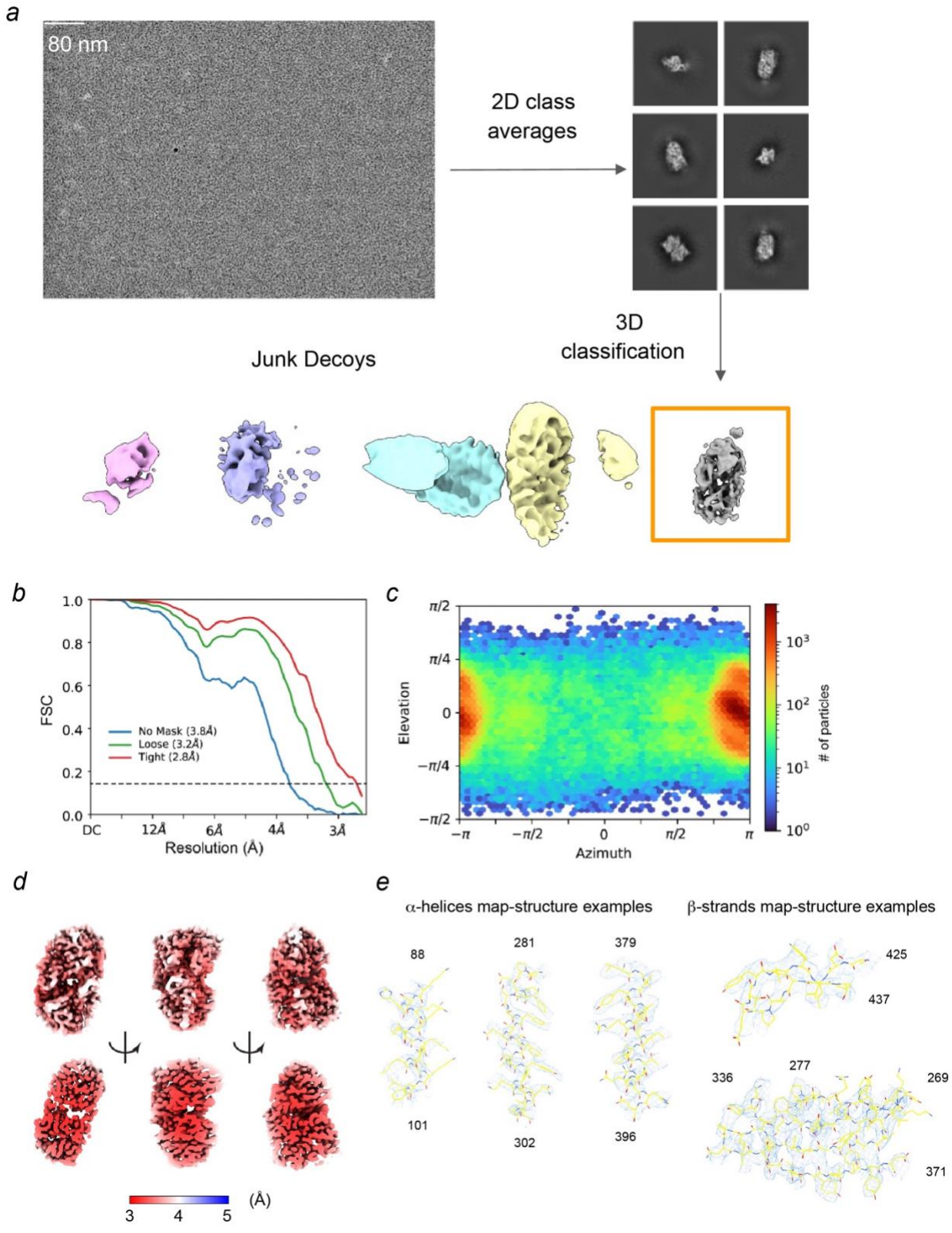
a
80 nm
2D class averages
3D classification
Junk Decoys
b
FSC
No Mask (3.8Å)
Loose (3.2Å)
Tight (2.8Å)
DC
12Å
6Å
4Å
3Å
Resolution (Å)
c
Elevation
Azimuth
# of particles
d
(Å)
e
α-helices map-structure examples
β-strands map-structure examples
88
101
281
302
379
396
425
437
277
336
269
371

Supplementary Figure 7. CryoEM image processing of hATE1 in apo state. (a) The image processing workflow. A representative micrograph of hATE1 cryo-grids was shown with representative 2D and 3D class averages. The scale bar is 80 nm. (b) FSC curve for 3D reconstruction maps of apo hATE1. The grey dash line indicates the 0.143 FSC cutoff. (c) Angular distribution of apo hATE1 particle set. (d) Local resolution of hATE1 displayed on the surface of the cryoEM map (top) and a plane slicing through the middle of the cryoEM map (bottom). The color code is shown in the color bar. (e) Maps for representative α-helices and β-strands shown individually with the structural model.

Suppl. Fig. 8

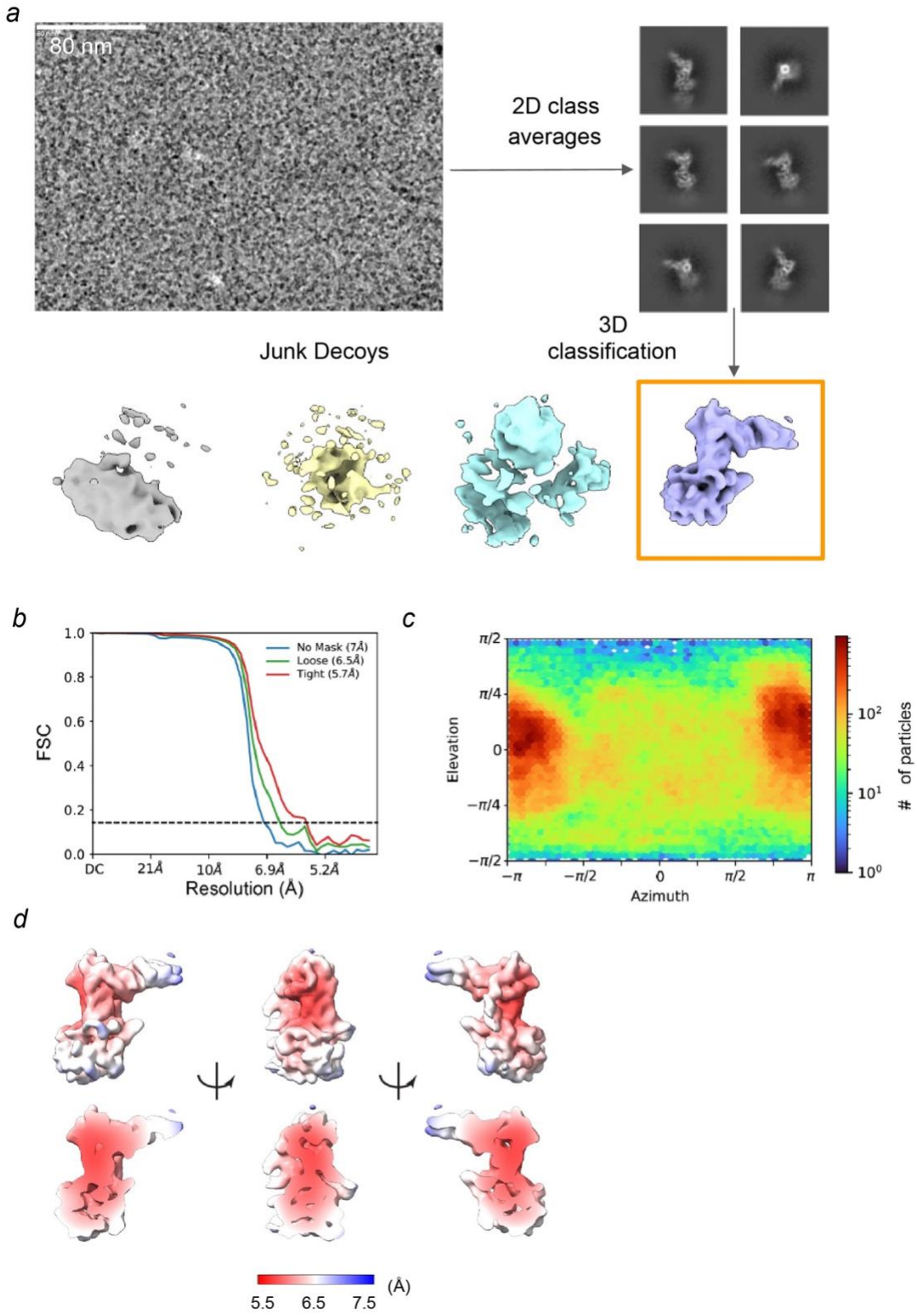
a
80 nm
2D class averages
3D classification
Junk Decoys
b
FSC
Resolution (Å)
No Mask (7Å)
Loose (6.5Å)
Tight (5.7Å)
DC
21Å
10Å
6.9Å
5.2Å
c
Elevation
Azimuth
# of particles
d
(Å)
5.5
6.5
7.5

Supplementary Figure 8. CryoEM image processing of hATE1•tRNA^{Arg}•substrate complex. (a) The image processing workflow. A representative micrograph of hATE1 cryo-grids was shown with representative 2D and 3D class averages. The scale bar is 80 nm. (b) FSC curve for 3D reconstruction maps of hATE1 complex. The grey dash line indicates the 0.143 FSC cutoff. (c) Angular distribution of hATE1 complex particle set. (d) Local resolution of hATE1•tRNA^{Arg} displayed on the surface of the cryoEM map (top) and a plane slicing through the middle of the cryoEM map (bottom).. The color code is shown in the color bar.

Supplementary Table 1. Data collection and refinement statics for the human ATE1.

	*hs*ATE1	*hs*ATE1/peptide/tRNA^{Arg}
Microscope	Titan Krios	
Voltage (keV)	300	
Image filter	BioQuantum	
Slit width (eV)	20	
Super-resolution Pixel size (Å)	0.67	0.26
Symmetry	C1	
Dofocus range (micron)	-0.5 to -2.5	
Electron dose (e^-/Å^2)	40	100
Micrographs	1,735	9,256
Number of particles	228,665	219,685
Map resolution at 0.143 FSC (Å)	2.8	5.7
B-factor	94.9	607.4
Model Refinement		
Atom	5,688	4,400
Residues	Protein: 698, Nucleotides: 0	Protein: 344, Nucleotides: 76
Ligands	ZN: 1	ZN: 1
CCmask	0.73	0.71
Resolution (FSC map vs. model at 0.5) (Å)	3.9	7.7
r.m.s. deviations		
Bond lengths (Å)	0.001	0.002
Bond angles (°)	0.399	0.581
Clash score	6.61	9.26
MolProbity score	1.36	2.75
PDB ID	8TZV	8UAU
EMDB ID	41770	42071